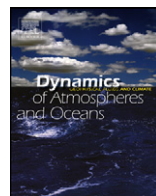




ELSEVIER

Contents lists available at ScienceDirect

Dynamics of Atmospheres and Oceans

journal homepage: www.elsevier.com/locate/dynatmoce

The role of mean ocean salinity in climate

Paul D. Williams^{a,*}, Eric Guilyardi^{a,b}, Gervan Madec^b, Silvio Gualdi^c,
Enrico Scoccimarro^c

^a National Centre for Atmospheric Science, Department of Meteorology, University of Reading, UK

^b Laboratoire d'Océanographie et de Climat: Expérimentation et Approche Numérique (LOCEAN/IPSL), CNRS/Université Paris VI, France

^c Istituto Nazionale di Geofisica e Vulcanologia, Bologna, Italy

ARTICLE INFO

Article history:

Received 17 October 2008

Received in revised form 4 February 2009

Accepted 4 February 2009

Available online 13 February 2009

Keywords:

Ocean

Salinity

Climate

Thermohaline circulation

THC

El Niño

ENSO

Global warming

Hypersaline

ABSTRACT

We describe numerical simulations designed to elucidate the role of mean ocean salinity in climate. Using a coupled atmosphere-ocean general circulation model, we study a 100-year sensitivity experiment in which the global-mean salinity is approximately doubled from its present observed value, by adding 35 psu everywhere in the ocean. The salinity increase produces a rapid global-mean sea-surface warming of 0.8 °C within a few years, caused by reduced vertical mixing associated with changes in cabbeling. The warming is followed by a gradual global-mean sea-surface cooling of 0.4 °C within a few decades, caused by an increase in the vertical (downward) component of the isopycnal diffusive heat flux. We find no evidence of impacts on the variability of the thermohaline circulation (THC) or El Niño/Southern Oscillation (ENSO). The mean strength of the Atlantic meridional overturning is reduced by 20% and the North Atlantic Deep Water penetrates less deeply. Nevertheless, our results dispute claims that higher salinities for the world ocean have profound consequences for the thermohaline circulation.

In additional experiments with doubled atmospheric carbon dioxide, we find that the amplitude and spatial pattern of the global warming signal are modified in the hypersaline ocean. In particular, the equilibrated global-mean sea-surface temperature increase caused by doubling carbon dioxide is reduced by 10%. We infer the existence of a non-linear interaction between the climate responses to modified carbon dioxide and modified salinity.

© 2009 Elsevier B.V. All rights reserved.

* Corresponding author at: Department of Meteorology, University of Reading, PO Box 243, Earley Gate, Reading RG6 6BB, UK. Tel.: +44 118 378 7901; fax: +44 118 378 8316.

E-mail address: p.d.williams@reading.ac.uk (P.D. Williams).

1. Introduction

Salinity is the ocean signature of the global water cycle (Schmitt, 1995). Salinity affects ocean circulation, stability and variability (e.g. Fedorov et al., 2004; Huang et al., 2005) and hence plays a major role in climate. The basic physical mechanisms in which salinity participates derive from its influence on ocean density. At high latitudes, salinity modifies the vertical convective stability and is a major factor in the density-driven global thermohaline circulation (Manabe and Stouffer, 1995; Oka and Hasumi, 2004; Swingedouw et al., 2007). Brine rejection associated with sea-ice formation also modifies the density structure (Martinson, 1990; Gordon, 1991; Martinson and Iannuzzi, 1998; Marsland and Wolff, 2001). At low latitudes, the effects of salinity are more subtle, but significant impacts may arise through its roles in the control of density surfaces and the formation of barrier layers (Vialard and Delecluse, 1998a,b; Maes et al., 2002, 2005). Salinity depends on the surface fresh water flux, which is predicted to intensify in response to increased greenhouse-gas forcing (Cubasch et al., 2001; Yang et al., 2003; Bosilovich et al., 2005; Held and Soden, 2006). Therefore, processes involving salinity may be influential in determining the future climate.

Observations have revealed large-scale salinity changes in each of the major ocean basins during recent decades. Large amounts of fresh water have been added to the northern North Atlantic Ocean since the mid-1960s (Curry and Mauritzen, 2005). A freshening of the eastern half of the North Atlantic subpolar gyre has been observed during the same period (Josey and Marsh, 2005). Curry et al. (2003) have reported a systematic freshening between the 1950s and the 1990s at both poleward ends of a 50°S–60°N transect through the western Atlantic Ocean, accompanied by a systematic salinification at low latitudes. The observed salinity increase in recent decades in the 20°N–50°N latitude band of the Atlantic ocean is attributable to human influence (Stott et al., 2008). Wong et al. (1999) have reported a large-scale freshening of intermediate waters in the Pacific and Indian Oceans between the period 1930–1980 and the period 1985–1994. Bindoff and McDougall (2000) have reported a basin-wide freshening of the Indian Ocean below the mixed layer in 1987 compared to the 1950s and 1960s. Lukas (2001) has reported a freshening of the upper thermocline in the North Pacific subtropical gyre between 1991 and 1997. Whether due to natural variability or an anthropogenic trend, the impact of these basin-scale salinity changes on ocean circulation, stability and variability remains poorly understood.

The change in globally-averaged salinity during recent decades has been small and is probably not measurable, although Antonov et al. (2002) attempt to quantify it. The change has been caused by the addition to the ocean of a few centimetres of fresh water from melting land ice and sea ice. On geological timescales, however, the mean salinity of the world ocean has varied widely. Some variations have been caused by changes in the total water content of the ocean, such as occurred during the large-scale extraction of water to form the Antarctic ice sheet. Other variations have been caused by changes in the total salt content. Salt from rocks is conveyed to the ocean by rivers, ground water and glaciers, and it is extracted from the ocean by the formation of evaporite salt deposits, of which there are many in the geological record. The input and extraction processes are not in instantaneous balance, however, and so the total global salt content may vary. Hay et al. (2006) have used data on the volumes and masses of evaporite deposits to construct a proxy record of the mean salinity of the ocean. They conclude that there have been significant changes in the mean salinity throughout the Phanerozoic eon (i.e. the most recent 545 million years). In particular, there were relatively few large extractions of salt during the early Palaeozoic era (i.e. the earliest era of the Phanerozoic eon), suggesting slowly increasing global-mean ocean salinities exceeding 50 psu.

Waters of salinity greater than 40 psu are referred to as hypersaline or hyperhaline. It has been suggested that such high salinities may have profound consequences for the thermohaline circulation of the past. For example, Hay et al. (2006) argue that at present observed salinities, the density of sea water is only slightly affected by cooling as the freezing point is approached, and so salinization (through sea-ice formation or evaporation) is generally required in order for deep convection to occur. At salinities above about 40 psu, however, water continues to become more dense as the freezing point is approached, and so salinization is no longer needed for deep convection. Therefore, the phase changes involved in sea-ice formation and evaporation, which consume energy and thereby reduce the deep water formation rate, are also no longer needed. Much less energy would be required to drive

the thermohaline circulation in a hypersaline ocean, argue Hay et al. (2006), because a hypersaline ocean could convect much more readily.

Despite the crucial importance of salinity, our understanding of the processes and feedbacks in which it participates remains incomplete. For example, several studies have suggested that anthropogenic warming could weaken the thermohaline circulation, by increasing the fresh water inputs, and reducing the surface salinity, at high latitudes (e.g. Wood et al., 1999; Thorpe et al., 2001). But current climate models differ widely in their thermohaline circulation response to greenhouse-gas forcing (Cubasch et al., 2001; Gregory et al., 2005). This divergence reflects the fact that, although the leading salinity processes have been identified – poleward advection of high-salinity waters, atmospheric water vapour transport, and high-latitude interaction with sea ice (e.g. Rahmstorf, 1996; Latif et al., 2000; Vellinga et al., 2002; Saenko et al., 2002; Dong and Sutton, 2002, 2005) – different models are dominated by different feedbacks between these processes. There is little consensus about which feedbacks are the most important and so it is unclear which of the thermohaline circulation projections is correct.

Some modelling studies have suggested that salinity plays a more dominant role in determining climate variability than it does in determining the mean climate. For example, in sensitivity experiments with homogeneous salinity, Vialard et al. (2002) find that the mean state of the equatorial Pacific Ocean is only weakly modified (by 0.2°C in surface temperature) but that the temporal standard deviation is strongly increased (by 0.4°C compared to a control value of 1°C). Thermohaline circulation simulations that distinguish the relative influences of the haline, thermal and momentum forcing also suggest that, although thermal forcing is the dominant driver of the mean thermohaline circulation, haline forcing is the dominant driver of its variability (e.g. Wang et al., 1999a,b; Saenko et al., 2002).

Williams et al. (2006) proposed a specific mechanism by which salinity may influence climate in tropical and sub-tropical regions. The net fresh water flux at the ocean surface maintains isopycnal salinity gradients, which must (by definition) be accompanied by density-compensating isopycnal temperature gradients. The concomitant isopycnal diffusive heat flux has a vertical component of around 1 W m^{-2} downwards at low and middle latitudes (Osborn, 1998). This heat flux enters into the mixed-layer heat budget and tends to cool the surface temperature. An anthropogenically-enhanced hydrological cycle would strengthen isopycnal salinity gradients, increasing this heat flux, producing an anomalous net downward transfer of heat, and cooling the surface. Therefore, this mechanism contributes a negative feedback to anthropogenic global warming. From a sensitivity experiment with doubled surface fresh water forcing, Williams et al. (2007) estimated that a 10% increase in the hydrological cycle would contribute a basin-scale equilibrium sea-surface temperature decrease of around 0.1°C within around a decade away from high latitudes, with larger decreases locally.

In this paper, we describe numerical simulations designed to help elucidate the role of mean ocean salinity in climate. Our intention is not to simulate directly a possible future or past climate. Rather, our intention is to study basic oceanic processes involving salinity. To achieve this goal, we perform sensitivity experiments in which the global-mean salinity is greatly increased from its present observed value. Our aim is to document the resulting climatic state and to understand the adjustment mechanisms by which it is reached. Process studies such as this are an attempt to learn something about the fundamental mechanisms that maintain realistic climates; they are not an attempt to simulate realistic climates explicitly.

The layout of this paper is as follows. Section 2 describes the coupled atmosphere-ocean general circulation model and the experiments performed. Section 3 examines the impacts of the increased salinity on the mean climate, by identifying two distinct mechanisms with which the ocean adjusts to the new salinity field. The response of the thermohaline circulation in the Atlantic Ocean is also examined. Section 4 studies the impacts on the climate response to doubled atmospheric carbon dioxide and Section 5 studies the impacts on climate variability. We summarize and discuss our findings in Section 6.

2. Methodology

We use the SINTEX-G atmosphere/ocean/sea-ice general circulation model developed at the Istituto Nazionale di Geofisica e Vulcanologia (INGV) in Bologna (Gualdi et al., 2008). The model is structurally

similar to the SINTEX atmosphere/ocean general circulation model (Guilyardi et al., 2003; Gualdi et al., 2003) from which it evolved. The main difference is that, instead of imposing relaxation towards climatological sea ice, SINTEX-G includes a comprehensive dynamic-thermodynamic sea-ice model, making it suitable for climate change experiments.

The ocean component of SINTEX-G is ORCA2, the global configuration of OPA8.2 (Madec et al., 1998). The model uses a finite difference scheme to integrate the hydrostatic primitive equations with a time step of 90 min. A tri-polar curvilinear mesh is used to avoid the North Pole singularity of geographical meshes (Murray, 1996; Madec and Imbard, 1996). The longitudinal resolution is 2.0° and the latitudinal resolution ranges from 0.5° at the equator to 2.0° at the poles. The vertical resolution ranges from 10 m near the surface to 500 m near the bottom. The model uses an implicit free surface formulation (Roulet and Madec, 2000) in which the depth of the top model layer may vary. Therefore, virtual salinity fluxes, which are required in rigid-lid models to ensure salt conservation, are not used. The density is computed using the UNESCO international equation of state for sea water, cast in the computationally efficient form of Jackett and McDougall (1995). The lateral mixing of temperature and salinity is quasi-pure isopycnal (Guilyardi et al., 2001). Eddy-induced velocities are parameterized using the Gent and McWilliams (1990) scheme except that, equatorwards of 20°N and 20°S , the Gent and McWilliams (1990) velocities are reduced in proportion to the ratio of the local Coriolis parameter to that at 20° . The sea-ice model is LIM (Fichefet and Morales Maqueda, 1997), which runs on the same tri-polar grid as the ocean model and uses the same time step. The atmosphere model is ECHAM4.6 (Roeckner et al., 1996), which integrates the primitive equations on a T30L19 grid with a time step of 30 min.

The ocean and sea-ice models are coupled every 90 min using the coupling strategy described by Timmermann et al. (2005). The ocean and sea-ice models are coupled to the atmosphere model every 180 min using OASIS2.4 (Valcke et al., 2000) and the coupling strategy described by Guilyardi et al. (2003). Temperature and salinity are relaxed towards the Levitus (1982) climatology in the Mediterranean Sea and the Red Sea, which are not well resolved. Apart from this, no flux adjustment is applied.

In the standard SINTEX-G model, the run-off of fresh water from the continents into the ocean is not derived from the integrated precipitation and evaporation over land, but instead follows a prescribed climatology. Therefore, the global water cycle is not closed. Since the feedback of modified run-off may influence salinity, especially in the North Atlantic Ocean, we developed a simple river catchment model for SINTEX-G before beginning our experiments. Each land point on the T30 atmosphere grid is assigned to one of 44 rivers, and each river is given a mouth on the ocean grid. Precipitation over any land point is instantly ejected into the ocean at the corresponding river mouth. Therefore, land hydrology (including soil moisture storage, evaporation from land, and the delays of river routing and snow cover melt) is absent from the model, but the global water cycle is closed, which is the leading requirement. The database of 44 catchments consists of the 35 largest rivers in the world (Hagemann and Dümenil, 1998), plus 8 catchments for Antarctica and 1 for Greenland.

We study four SINTEX-G integrations in this paper, each 100 years long. The control simulation (hereafter referred to as **CTRL**) is initiated from an ocean with the observed three-dimensional thermohaline structure of Levitus (1982). The century-mean ocean state in **CTRL** compares well with the Levitus (1982) data, indicating that SINTEX-G faithfully captures the observed mean climate. The main perturbation simulation (hereafter **HIGHSAL**) is identical except that 35 psu is added to the salinity at each ocean grid point in the three-dimensional initial state (and also to the Mediterranean Sea and Red Sea relaxation salinities). Since the global-mean ocean salinity in **CTRL** is 34.7 psu, the global-mean salinity in **HIGHSAL** is approximately double that in **CTRL**. We choose such a high salinity in order to magnify the effects we are interested in and produce a clear response. We assume that the equation of state applies outside the calibrated salinity range of 0–42 psu. As justification for this assumption¹, we note that Spigel and Prisco (1996) have measured densities in a hypersaline Antarctic lake, and have

¹ As further justification, a reviewer has noted that a new equation of state is due in 2010, that will extend the salinity range up to 120 psu and confirm the linearity of the haline contraction parameter over the range of salinities considered here.

calculated that the UNESCO international equation of state is in error by at most 5 kg m^{-3} for salinities in the range 42–80 psu (see their Fig. 5).

In **CTRL** and **HIGHSAL**, the atmospheric carbon dioxide concentration is held fixed at 353 ppm, which is the observed 1990 value. Two further simulations (hereafter **2CO2** and **HIGHSAL_2CO2**) are identical to **CTRL** and **HIGHSAL**, respectively, except that the atmospheric carbon dioxide concentration is held fixed at 706 ppm, which is twice the control value. Our motivation for the greenhouse-gas simulations is a desire to investigate how the climate responses to modified oceanic salinity and modified atmospheric carbon dioxide interact. In particular, would anthropogenic global warming be different in a world with a hypersaline ocean?

3. Impacts on the mean climate

In this section, we compare the ocean states in **CTRL** and **HIGHSAL**, first at high latitudes (Section 3.1) and then globally at the surface (Section 3.2) and in the interior (Section 3.3). We also compare the thermohaline circulations in the Atlantic Ocean (Section 3.4).

3.1. High latitudes

Antarctic sea ice is unstable in **HIGHSAL**. The ice forms normally in the first southern-hemisphere winter but fails to form in the second winter (and in all subsequent winters). Arctic sea ice is stable but its extent is reduced slightly during the first few decades. Sea ice in SINTEX-G is evidently very sensitive: one of us (SG) worked on increasing the atmospheric resolution from T30 to T106 and recalls that much parameter tuning was required to produce stable sea ice.

One possible explanation for the unstable sea ice in **HIGHSAL** is that adding 35 psu reduces the freezing point of sea water from around -2°C to around -4°C . Therefore, mixed-layer water under sea ice in **HIGHSAL** is initially 2°C above the freezing point, and it could be that the atmosphere cannot extract heat from the ocean rapidly enough to cool it to the freezing point. For example, to cool a mixed layer of depth 50 m by 2°C in 6 months requires an additional 30 W m^{-2} of heat to be extracted. However, this explanation seems unlikely, because the surface air temperature is still lower than the ocean freezing point temperature. It is more likely that thermobaric convection is preventing the sea ice from growing back: any cooling at the surface will lead to an instability and subsequent mixing of that cooled water through the entire water column.

We tried various modifications to **HIGHSAL**, to see if it was possible to retain Antarctic sea ice. First, we tried adding the 35 psu on 1 July rather than 1 January, so that the southern hemisphere ice extent was already at its maximum when the perturbation was introduced. Second, as well as adding 35 psu, we tried setting the mixed-layer temperature under sea ice equal to the freezing point calculated using the new local salinity (which produced a mean change of around -2°C) and co-modifying the salinity such that the density was unaltered (which produced a mean change of around -0.1 psu). Neither of these modifications produced stable Antarctic sea ice. We conclude that Antarctic sea ice is physically unstable in this model when ocean salinity is increased by 35 psu, and we proceed by accepting that it must melt permanently in **HIGHSAL**. The particular **HIGHSAL** simulation studied in this paper uses both of the above modifications, but none of our findings is sensitive to this choice.

3.2. The ocean surface

Fig. 1 shows time series of global-mean annual-mean sea-surface temperature, for each experiment and for differences between experiments. After a transient adjustment to the *Levitus (1982)* initial conditions in the first few years, **CTRL** reaches a stable equilibrium value of 20.0°C with superimposed inter-annual variability. By the end of the integrations, **HIGHSAL** has warmed relative to **CTRL** by 0.4°C . The warming is clearly statistically significant compared to the inter-annual variability. The net anomalous warming in **HIGHSAL** is achieved through a rapid warming by 0.8°C during the first few years, followed by a gradual cooling by 0.4°C during the first few decades. Stabilisation is reached after 30–40 years. The rapid warming and gradual cooling suggest two distinct adjustment mechanisms by which **HIGHSAL** responds to the increased salinity.

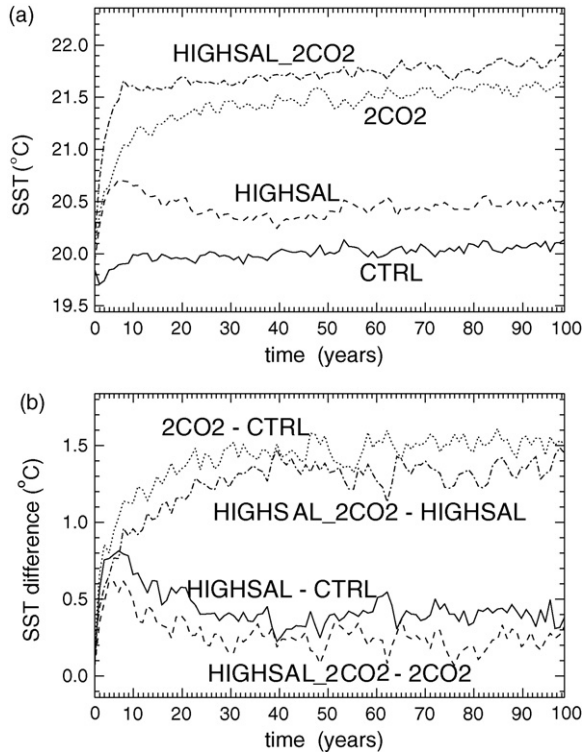


Fig. 1. (a) Global-mean annual-mean sea-surface temperature (SST) in each experiment. The corresponding time series of global-mean annual-mean sea-surface salinity (not shown) exhibit linear drifts of +0.3 psu/century in **CTRL** and **2CO2** and +0.6 psu/century in **HIGHSAL** and **HIGHSAL_2CO2**, which are small for a coupled model without flux adjustment. (b) Selected differences between the curves in (a).

The initial rapid anomalous sea-surface warming in **HIGHSAL** is caused by vertical adjustment due to cabbeling, as illustrated in Fig. 2. Cabbeling refers to the slight density increase that results when two fluid parcels of the same density, but different temperatures and salinities, are mixed. The densification upon mixing occurs because the thermal and haline expansion coefficients of sea water depend upon temperature and salinity, producing non-linearities in the equation of state and giving curvature to constant-density contours in the temperature-salinity plane. The denser water that results from isopycnal mixing is convectively unstable and causes rapid vertical mixing. This process occurs in both **CTRL** and **HIGHSAL**, but the non-linearities in the equation of state are weaker at the typical salinities encountered in **HIGHSAL**. Therefore, the density increases caused by cabbeling are smaller in **HIGHSAL** than in **CTRL**, reducing the vertical mixing, increasing the stratification, and rapidly warming the surface.

For the purposes of interpreting the subsequent gradual anomalous sea-surface cooling in **HIGHSAL**, it is instructive to consider how increased salinity affects the ocean’s response to surface fresh water forcing. For an ocean of sea-surface salinity S , let the sea-surface salinity change that results from a given surface fresh water exchange be ΔS . Then it follows from salt conservation that the corresponding change, $\Delta S_{+35 \text{ psu}}$, for an ocean of sea-surface salinity $S+35$ psu subjected to the same fresh water exchange, is given by

$$\Delta S_{+35 \text{ psu}} = \frac{S + 35 \text{ psu}}{S} \Delta S. \tag{1}$$

We conclude that adding 35 psu causes the sea-surface salinity change inflicted by surface fresh water fluxes to be multiplied by a salinity-dependent factor greater than 1. For example, water of sea-

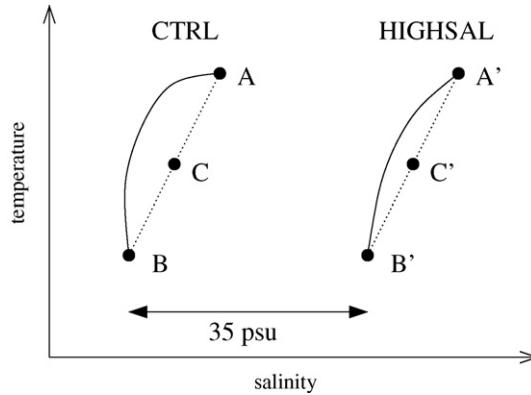


Fig. 2. Schematic comparison of the cabelling mechanism in **CTRL** and **HIGHSAL**. The curvature of constant-density contours in the temperature-salinity plane (shown as solid lines) decreases with increasing salinity (shown exaggerated). Therefore, the amount by which the density of the water formed from cabelling (C) exceeds the density of the parent waters (A and B) is greater in **CTRL** than in **HIGHSAL**.

surface salinity 70 psu experiences twice the salinity change of water of sea-surface salinity 35 psu. Therefore, the role of salinity is magnified in **HIGHSAL** compared to **CTRL** (and in **HIGHSAL.2CO2** compared to **2CO2**). The amplification factor, $(S + 35 \text{ psu})/S$, is plotted as a function of S in Fig. 3. The spatial structure of the amplification factor, calculated from observations of sea-surface salinity, is plotted in Fig. 4. For the physical range of sea-surface salinities observed in the ocean (around 25–40 psu), the amplification factor ranges from around 1.9 to 2.4. For the mean sea-surface salinity (around 35 psu), the amplification factor is 2.0. Note that the amplification factor may alternatively be interpreted as the factor by which the effective surface fresh water flux is multiplied. Specifically, water of sea-surface salinity $S + 35 \text{ psu}$ subjected to a surface fresh water flux F experiences the same salinity change as water of sea-surface salinity S subjected to a surface fresh water flux $F_{+35 \text{ psu}}^{\text{effective}}$.

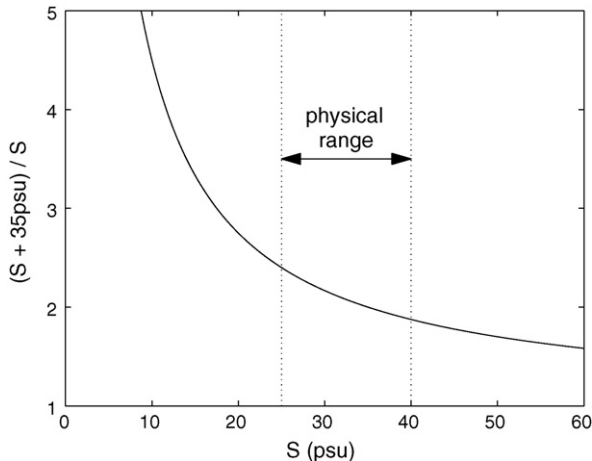


Fig. 3. Amplification factor in Eqs. (1) and (2) plotted as a function of sea-surface salinity. The amplification factor is the amount by which the sea-surface salinity change inflicted by surface fresh water exchanges is multiplied when the salinity is increased by 35 psu, or alternatively the amount by which the effective surface fresh water flux is multiplied (see text). The approximate physical range of sea-surface salinities observed in the ocean is indicated: salinities near 25 psu are found in Hudson Bay and salinities near 40 psu are found in the Mediterranean Sea and Red Sea (see Fig. 4(a)).

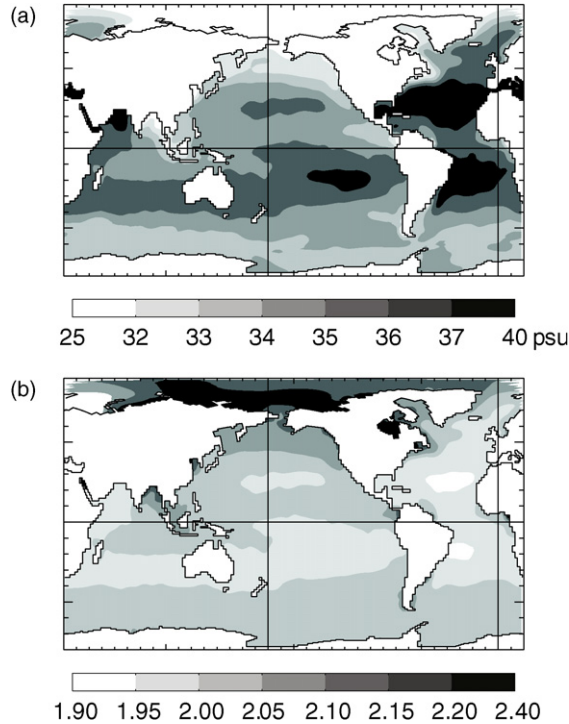


Fig. 4. (a) Sea-surface salinity according to the Levitus (1982) observations. (b) Amplification factor calculated by projecting (a) onto the curve of Fig. 3.

given by

$$F_{+35 \text{ psu}}^{\text{effective}} = \frac{S + 35 \text{ psu}}{S} F. \quad (2)$$

The effective surface fresh water flux amplification provides a bridge to our previous work on the effects of modified surface fresh water forcing (Williams et al., 2006, 2007). In particular, the gradual anomalous sea-surface cooling in **HIGHSAL** is caused by the adjustment mechanism operating in the doubled hydrological cycle experiment of Williams et al. (2007), which was described in Section 1 and has a decadal timescale. The surface fresh water forcing is effectively amplified by the increased mean salinity. Therefore, isopycnal salinity and temperature gradients are amplified, intensifying the isopycnal diffusive heat flux (see Williams et al., 2006, for further details). As evidence to support this claim, Fig. 5 shows profiles of the vertical component of the isopycnal diffusive heat flux in the Pacific Ocean of **HIGHSAL**. The flux is directed downwards and increases by around 10% over most of the upper 1000 m between the second and fourth decades, cooling the surface and causing heat to be stored at depth. The corresponding heat flux profiles in the Atlantic Ocean are similar (not shown).

The pattern of anomalous sea-surface temperature change in **HIGHSAL** between the second and fourth decades is shown in Fig. 6. This particular time difference exposes the fingerprint of the slow mechanism and isolates it from that of the fast mechanism. In terms of the general cooling at low and middle latitudes, the pattern qualitatively resembles that seen in the doubled hydrological cycle experiment of Williams et al. (2007). The resemblance is poor at high latitudes (e.g., the far North Pacific and the Ross Sea) due to sea-ice effects (Section 3.1), which are absent in the Williams et al. (2007) experiment because of relaxation towards climatological sea ice. The approximate latitudes of the areas influenced by the sea ice are those polewards of 50°N and 60°S.

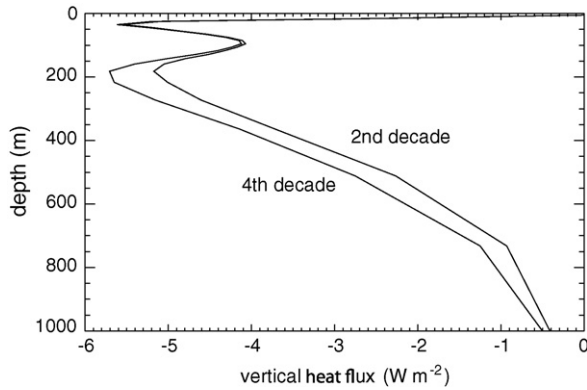


Fig. 5. Vertical profiles of the vertical component of the isopycnal diffusive heat flux in **HIGHSAL**, averaged in the Pacific Ocean (40°N – 40°S and 110°E – 70°W) over the second decade (years 11–20) and the fourth decade (years 31–40). Negative values indicate a downward flux.

3.3. The ocean interior

The vertical profile of global-mean anomalous temperature change in **HIGHSAL** between the second and fourth decades is shown in Fig. 7. Once again, we choose this particular time difference because it exposes the slow adjustment mechanism. The global surface cooling seen in Fig. 6 extends down to around 100 m and is accompanied by a warming of the depth range 100–650 m. The sub-surface warming reaches 0.3°C near 400 m. The vertical profile strongly resembles that seen in the doubled hydrological cycle experiment of Williams et al. (2007) and is caused by a net downward heat transfer due to the increased isopycnal diffusive heat flux.

3.4. The Atlantic Ocean thermohaline circulation

Fig. 8 (a) shows the simulated Atlantic meridional overturning stream function at the end of **CTRL**. The overturning consists of a warm northward branch in the upper 1000 m and a cold deep return flow composed of North Atlantic Deep Water (NADW). Most of the NADW is formed in the Greenland, Iceland, Norwegian and Labrador seas in the high-latitude North Atlantic. In these regional seas, the surface waters are cool (because of heat loss to the atmosphere) and saline (because the Atlantic is a net evaporative basin) and so they are dense and sink as NADW. At middle latitudes in the northern

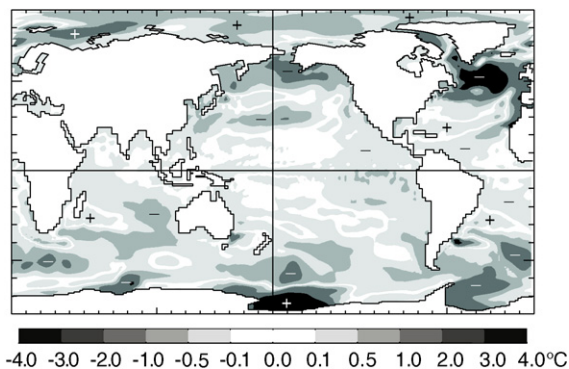


Fig. 6. Change, between averages over the second decade (years 11–20) and the fourth decade (years 31–40), in the sea-surface temperature of **HIGHSAL** relative to **CTRL**. Note the qualitative resemblance with the top panel of Fig. 2 of Williams et al. (2007). Positive (+) and negative (–) regions are indicated.

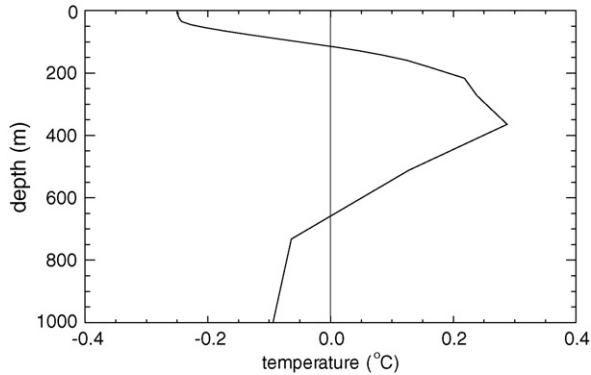


Fig. 7. Change, between averages over the second decade (years 11–20) and the fourth decade (years 31–40), in the global-mean ocean temperature profile of **HIGSAL** relative to **CTRL**. Note the strong qualitative resemblance with the middle panel of Fig. 2 of Williams et al. (2007).

hemisphere, northward-flowing Antarctic Bottom Water (AABW) converges with southward-flowing Denmark Strait Overflow Water (DSOW) near the ocean floor, and upwells into the southward-flowing NADW. This deep recirculation is seen in Fig. 8(a) as the region of small positive stream function centred near 15°N and 4000 m.

The simulated Atlantic meridional overturning stream function at the end of **HIGSAL** is shown in Fig. 8(b), and the anomaly with respect to **CTRL** is shown in Fig. 8(c). Note that the deep ocean is unlikely

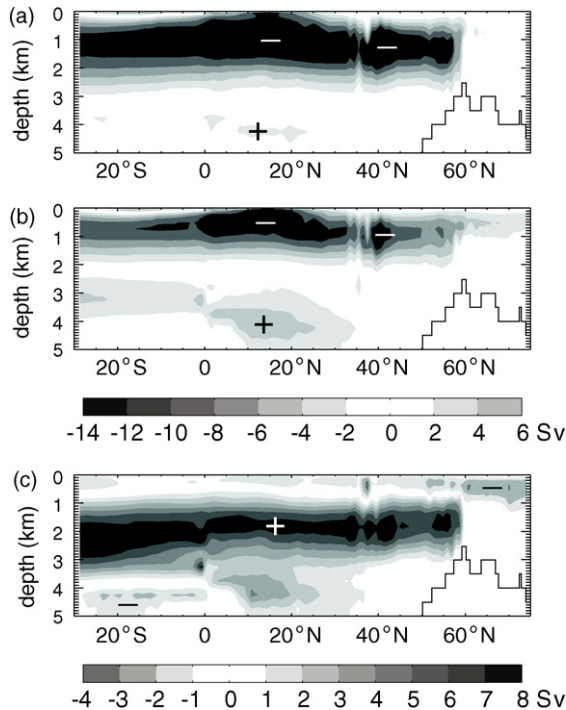


Fig. 8. Atlantic meridional overturning stream function averaged over the final decade (years 91–100) in (a) **CTRL** and (b) **HIGSAL**. Negative values (–) indicate a clockwise circulation and positive values (+) indicate an anti-clockwise circulation. (c) shows (b) – (a). 1 Sv = $10^6 \text{ m}^3 \text{ s}^{-1}$.

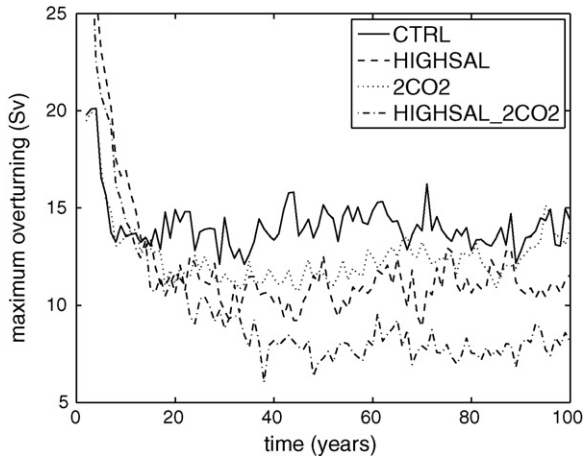


Fig. 9. Time series of the maximum of the annual-mean Atlantic meridional stream function north of 40°N in each experiment.

to be in equilibrium after only 100 years. The main impact of increasing the mean ocean salinity is to have raised the NADW to a higher level in the ocean. This rise occurs because saltier water is less compressible, as manifest by non-linearities in the equation of state associated with thermobaricity. Sinking parcels tend to increase in density as they fall, because they are compressible and the ambient pressure increases with depth. But parcel densities increase less rapidly with depth in **HIGHSAL** than in **CTRL**, because parcels in **HIGHSAL** are saltier and less compressible. Therefore, the level of neutral buoyancy, at which the sinking terminates and the NADW flows southwards, is shallower in **HIGHSAL** than in **CTRL**.

There are three other noteworthy features in Fig. 8(c). First, the overturning in the Nordic (Greenland, Iceland and Norwegian) seas, which are north of 60°N, increases by over 2 Sv in **HIGHSAL**. This increased meridional fluid exchange implies more communication between the Nordic seas and the North Atlantic ocean. Second, the deep recirculation caused by the mid-latitude convergence of AABW and DSOW increases by over 3 Sv, implying that the formation of AABW has increased in **HIGHSAL**. Finally, the shallow tropical-subtropical overturning cells, which consist of the upwelling of colder sub-surface waters at the equator and Ekman transport to higher latitudes, are essentially unaltered because they are wind-driven.

Fig. 9 shows time series of the maximum of the annual-mean Atlantic meridional stream function north of 40°N in each experiment. After a transient initial-condition adjustment in the first decade, **CTRL** reaches a mean overturning of 14.0 Sv (taken over years 30–100), which is within the observed range. After a larger and longer initial-condition adjustment to the new salinity field, during which the overturning exceeds 30 Sv in year 3, **HIGHSAL** reaches a mean overturning of 10.9 Sv (also taken over years 30–100). Therefore, the mean post-transient overturning in **HIGHSAL** is reduced by around 3 Sv compared to **CTRL**. This reduction is significant at the 99% level according to a two-tailed *t*-test. We conclude that doubling the mean ocean salinity reduces the strength of the Atlantic thermohaline circulation by around 20% in this model.

4. Impacts on climate response to doubled carbon dioxide

We now examine the two additional SINTEX-G experiments, **2CO2** and **HIGHSAL_2CO2**, which have twice the atmospheric carbon dioxide concentration of **CTRL** and **HIGHSAL** but are otherwise identical. We recall Fig. 1, which shows time series of global-mean annual-mean sea-surface temperature in all four experiments. The initial rapid warming and subsequent decadal cooling seen in **HIGHSAL** relative to **CTRL** are also seen in **HIGHSAL_2CO2** relative to **2CO2** (Fig. 1b). However, the final mean warming

(taken over years 30–100) caused by the salinity increase is reduced from 0.39°C with the control carbon dioxide to 0.23°C with doubled carbon dioxide. This reduction is significant at the 99% level according to a two-tailed t -test. Also, the global-mean sea-surface temperature increase (averaged over years 30–100) caused by doubling carbon dioxide is reduced from 1.49°C with the control salinity to 1.33°C with salinity increased by 35 psu. This 10% reduction is significant at the 99% level according to a two-tailed t -test.

We also recall Fig. 9, which shows time series of the maximum of the annual-mean Atlantic meridional stream function north of 40°N in all four experiments. The overturning in **2CO2** closely follows that in **CTRL** for around the first two decades, before the former weakens due to the increased high-latitude fresh water inputs associated with global warming. The same statement holds for **HIGHSAL 2CO2** and **HIGHSAL. 2CO2** and **HIGHSAL. 2CO2** reach mean overturnings of 12.2 and 8.0 Sv, respectively (taken over years 30–100). Therefore, the reduction in overturning caused by the salinity increase is increased from 3.1 Sv with the control carbon dioxide (Section 3.4) to 4.2 Sv with doubled carbon dioxide. This reduction is significant at the 99% level according to a two-tailed t -test.

Fig. 10 shows the spatial pattern of the equilibrated warming signal in the control and hypersaline oceans. If there were no interaction between the climate response to increased carbon dioxide and the climate response to increased mean salinity, then these two patterns would be identical and their difference, plotted in Fig. 10(c), would be zero everywhere. The differences at low and middle latitudes are very small, implying a negligible interaction despite the massive salinity perturbation applied. Larger differences are present at higher latitudes, indicating the presence of high-latitude non-linear interactions between the climate responses to modified oceanic salinity and modified atmospheric carbon dioxide.

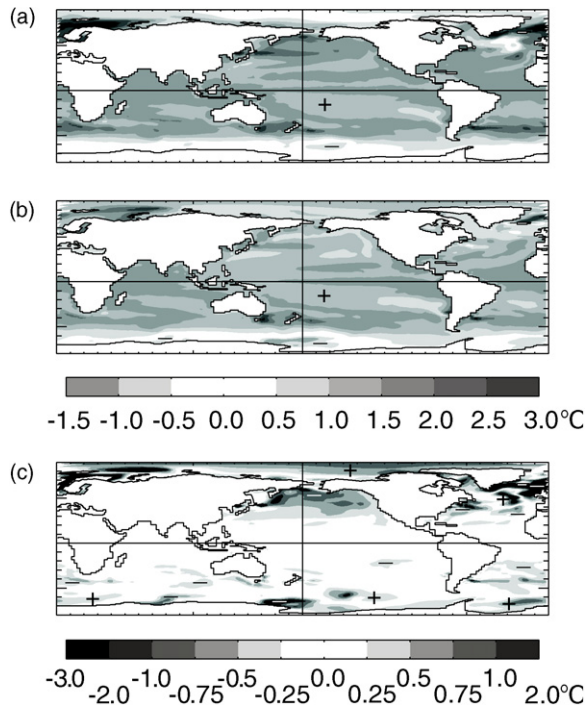


Fig. 10. Sea-surface temperature averaged over years 31–100 in (a) **2CO2** relative to **CTRL**, and (b) **HIGHSAL.2CO2** relative to **HIGHSAL.** (c) shows (b) – (a). Positive (+) and negative (–) regions are indicated.

5. Impacts on climate variability

We finally examine the impacts of the increased mean salinity on the climate variability. From Fig. 9, the standard deviation of the annual-mean Atlantic meridional overturning circulation over years 30–100 is 0.86 Sv in **CTRL**, 0.91 Sv in **HIGHSAL**, 0.91 Sv in **2CO2**, and 0.71 Sv in **HIGHSAL 2CO2**. There are no significant differences between these values. Specifically, pairs of two-tailed *F*-tests at the 99% significance level fail to reject the null hypothesis that the four populations from which these samples are drawn have identical standard deviations. We conclude that the inter-annual variability of the thermohaline circulation is not sensitive to the mean ocean salinity, at least in this model.

We reach the same conclusion regarding variability due to the El Niño/Southern Oscillation (ENSO). Specifically, the departure of monthly-mean sea-surface temperature in the Niño-3 region (150°W–90°W and 5°S–5°N) from the mean seasonal cycle over years 31–100, has the same standard deviation in **CTRL** and **HIGHSAL**. We also mention here the possibility of changed teleconnections due to the increased mean salinity. It is possible in principle to have changed teleconnections without any change in the mean climate, and so our analysis so far does not rule them out. However, maps (not shown) of the correlation of sea-surface temperature with the Niño-3 sea-surface temperature (at zero time-lag) reveal no significant difference between **CTRL** and **HIGHSAL**, indicating that ENSO teleconnections are unchanged.

The only incidence of changed variability we have been able to find is in the Nordic seas. For example, the departure of monthly-mean Iceland Sea sea-surface temperature from the mean seasonal cycle over years 31–100, has a standard deviation (taken over the same period) of 0.8 °C in **CTRL** and 1.6 °C in **HIGHSAL**. We speculate that this increased intra-annual variability is caused by the slight reduction in Arctic sea-ice extent (Section 3.1), which gives more scope for intra-annual variability in air-sea fluxes to influence the ocean state in the Nordic seas.

6. Summary and discussion

We have described numerical simulations designed to help elucidate the role of mean ocean salinity in climate. Using the SINTEX-G atmosphere/ocean/sea-ice general circulation model, we have studied 100-year sensitivity experiments in which the global-mean salinity is approximately doubled from its present observed value by adding 35 psu everywhere. This salinity increase amplifies the sea-surface salinity change inflicted by surface fresh water exchanges, and so is equivalent to amplifying the surface fresh water flux. Our study is motivated by predictions that the hydrological cycle will intensify under global warming; by observations of large-scale salinity changes in each of the major ocean basins during recent decades; by proxy evidence that the mean salinity of the world ocean has varied widely on geological timescales; and by a desire to test speculations that salinity might play a more dominant role in climate variability than in mean climate.

In our simulations, adding 35 psu produces a rapid global-mean sea-surface warming of 0.8 °C within a few years, caused by reduced vertical mixing associated with changes in cabbeling. The warming is followed by a gradual global-mean sea-surface cooling of 0.4 °C within a few decades. The cooling is caused by the mechanism of Williams et al. (2006, 2007): the effectively-amplified surface fresh water flux increases surface and isopycnal salinity gradients, which at low and middle latitudes increases the (downward) isopycnal diffusive heat flux, cooling the surface and causing heat to be stored at depth. Adding 35 psu destabilises sea ice, probably by a thermobaric convection mechanism. Adding 35 psu also reduces the annual-mean overturning north of 40°N in the Atlantic by 20%, and produces shallower North Atlantic Deep Water because saltier water is less compressible.

In additional experiments with doubled atmospheric carbon dioxide, we find that the amplitude and spatial pattern of the high-latitude global warming signal are modified in the hypersaline ocean. In particular, the equilibrated global-mean sea-surface temperature increase caused by doubling carbon dioxide is reduced by 10%. These changes imply the existence of a high-latitude non-linear interaction between the climate response to increased carbon dioxide and the climate response to increased mean salinity.

We find no evidence that the inter-annual variability of the Atlantic thermohaline circulation is modified in the hypersaline ocean. This finding disputes speculations that salinity, rather than tem-

perature, is the dominant driver of thermohaline circulation variability. Variability due to the El Niño/Southern Oscillation (ENSO) is also unmodified, contrary to suggestions (e.g. Vialard et al., 2002) that the variability in the equatorial Pacific Ocean is more sensitive to salinity than the mean is, but consistent with the findings of Williams et al. (2006). We find no evidence of modified ENSO teleconnections in response to the doubled salinity. Intra-annual variability of sea-surface temperature in the Nordic seas is significantly increased, but our results dispute the claim by Hay et al. (2006) that higher salinities for the world ocean have profound consequences for the thermohaline circulation of the past. The claim by Hay et al. (2006) appears to be disputed by other studies as well as ours. For example, the passive salinity experiment of Saenko et al. (2002) still exhibits convection and deep water formation in the North Atlantic.

There are three physical differences between the doubled hydrological cycle experiment of Williams et al. (2007) and the present hypersalinity experiments. First, the factor by which the (effective) surface fresh water flux is multiplied here is not identically 2 everywhere, but ranges from around 1.9 to 2.4. We expect (and find) this to result in some quantitative differences between the impacts in the two studies, but not to modify the overall qualitative findings. Second, the ocean equation of state is evaluated at higher salinities here, where non-linearities are weaker and isopycnals in the temperature-salinity plane are less curved. Finally, the present study uses an interactive sea-ice model rather than relaxation towards climatological sea ice. Therefore, we expect (and find) the qualitative evolution of the present raised salinity experiments to be explainable in terms of the Williams et al. (2007) adjustment mechanism, plus effects due to sea ice and non-linearities in the equation of state (i.e. cabbeling and thermobaricity).

This study advances the understanding of the climate response to an increased hydrological cycle beyond Williams et al. (2007) in three ways. First, Williams et al. (2007) looked only at the climatic impacts at low latitudes, because their model used relaxation to climatological sea ice. This ruled out studying the thermohaline circulation. The present study uses a model with a fully interactive sea-ice scheme, allowing the global climatic impacts and thermohaline circulation to be assessed. Second, the approach taken in the present study is more physically consistent than the Williams et al. (2007) approach, in which the coupler artificially doubled the fresh water flux during coupling time steps. Third, the initial rapid surface warming seen in the present study, caused by vertical adjustment due to cabbeling, is not present in Williams et al. (2007).

The robustness of our findings could be assessed by repeating our experiments using other coupled general circulation models. It would be of particular interest to determine whether the instability of Antarctic sea ice in the hypersaline ocean is robust, or merely peculiar to the model we have used. We leave this for future work.

Acknowledgments

We thank Annalisa Cherchi at the Istituto Nazionale di Geofisica e Vulcanologia (INGV) in Bologna for her assistance and hospitality during PDW's visit to install SINTEX-G. We thank Olivier Marti at the Laboratoire des Sciences du Climat et de l'Environnement (LSCE) in Paris for his assistance with the MOZAIC interpolation software. We thank Jonathan Gregory for helpful comments on an early draft of this paper. We thank two anonymous reviewers for their constructive comments. Calculations were performed on the NEC SX-8 at the Institut du Développement et des Ressources en Informatique Scientifique (IDRIS/CNRS) in Paris and on the NEC SX-6 at the Deutsches Klimarechenzentrum (DKRZ/MPI-M) in Hamburg. We acknowledge funding from the Rapid Climate Change thematic programme of the UK Natural Environment Research Council (reference: NER/T/S/2002/00442). PDW is funded through a Fellowship from the UK Natural Environment Research Council (reference: NE/D009138/1).

References

- Antonov, J.I., Levitus, S., Boyer, T.P., 2002. Steric sea level variations during 1957–1994 importance of salinity. *J. Geophys. Res.* 107 (C12), 8013.
- Bindoff, N.L., McDougall, T.J., 2000. Decadal changes along an Indian ocean section at 32°S and their interpretation. *J. Phys. Oceanogr.* 30, 1207–1222.
- Bosilovich, M.G., Schubert, S.D., Walker, G.K., 2005. Global changes of the water cycle intensity. *J. Clim.* 18 (10), 1591–1608.

- Cubasch, U., Meehl, G.A., Boer, G.J., Stouffer, R.J., Dix, M., Noda, A., Senior, C.A., Raper, S.C.B., Yap, K.S., 2001. Projections of future climate change. In: Houghton, J.T., Ding, Y., Griggs, D.J., Noguer, M., van der Linden, P., Dai, X., Maskell, K., Johnson, C.I. (Eds.), *Climate Change 2001: The Scientific Basis*. Contribution of Working Group I to the Third Assessment Report of the Intergovernmental Panel on Climate Change. Cambridge University Press, pp. 525–582.
- Curry, R., Mauritzen, C., 2005. Dilution of the Northern North Atlantic ocean in recent decades. *Science* 308, 1772–1774.
- Curry, R., Dickson, B., Yashayaev, I., 2003. A change in the freshwater balance of the Atlantic Ocean over the past four decades. *Nature* 426, 826–829.
- Dong, B., Sutton, R., 2002. Adjustment of the coupled ocean–atmosphere system to a sudden change in the thermohaline circulation. *Geophys. Res. Lett.* 29 (15), 1728.
- Dong, B., Sutton, R.T., 2005. Mechanism of interdecadal thermohaline circulation variability in a coupled ocean–atmosphere GCM. *J. Clim.* 18, 1117–1135.
- Fedorov, A.V., Pacanowski, R.C., Philander, S.G., Boccaletti, G., 2004. The effect of salinity on the wind-driven circulation and the thermal structure of the upper ocean. *J. Phys. Oceanogr.* 34, 1949–1966.
- Fichefet, T., Morales Maqueda, M.A., 1997. Sensitivity of a global sea ice model to the treatment of ice thermodynamics and dynamics. *J. Geophys. Res.* 102 (C6), 12609–12646.
- Gent, P.R., McWilliams, J.C., 1990. Isopycnal mixing in ocean circulation models. *J. Phys. Oceanogr.* 20, 150–155.
- Gordon, A.L., 1991. Two stable modes of Southern Ocean winter stratification. In: *Deep Convection and Deep Water Formation in the Oceans*, volume 57 of Elsevier Oceanography Series, Elsevier, pp. 17–35.
- Gregory, J.M., Dixon, K.W., Stouffer, R.J., Weaver, A.J., Driesschaert, E., Eby, M., Fichefet, T., Hasumi, H., Hu, A., Jungclaus, J.H., Kamenkovich, I.V., Levermann, A., Montoya, M., Murakami, S., Nawrath, S., Oka, A., Sokolov, A.P., Thorpe, R.B., 2005. A model intercomparison of changes in the Atlantic thermohaline circulation in response to increasing atmospheric CO₂ concentration. *Geophys. Res. Lett.* 32, L12703.
- Gualdi, S., Navarra, A., Guilyardi, E., Delecluse, P., 2003. Assessment of the tropical Indo-Pacific climate in the SINTEX CGCM. *Ann. Geophys.* 46 (1), 1–26.
- Gualdi, S., Scoccimarro, E., Navarra, A., 2008. Changes in tropical cyclone activity due to global warming: results from a high-resolution coupled general circulation model. *J. Clim.* 21 (20), 5204–5228.
- Guilyardi, E., Madec, G., Terray, L., 2001. The role of lateral ocean physics in the upper ocean thermal balance of a coupled ocean–atmosphere GCM. *Clim. Dyn.* 17 (8), 589–599.
- Guilyardi, E., Delecluse, P., Gualdi, S., Navarra, A., 2003. Mechanisms for ENSO phase change in a coupled GCM. *J. Clim.* 16, 1141–1158.
- Hagemann, S., Dümenil, L., 1998. A parametrization of the lateral water flow for the global scale. *Clim. Dyn.* 14 (1), 17–31.
- Hay, W.W., Migdisov, A., Balukhovskiy, A.N., Wold, C.N., Fogel, S., Soding, E., 2006. Evaporites and the salinity of the ocean during the Phanerozoic: implications for climate, ocean circulation and life. *Palaeogeogr. Palaeoclimatol. Palaeoecol.* 240, 3–46.
- Held, I.M., Soden, B.J., 2006. Robust responses of the hydrological cycle to global warming. *J. Clim.* 19 (21), 5686–5699.
- Huang, B., Mehta, V.M., Schneider, N., 2005. Oceanic response to idealized net atmospheric freshwater in the Pacific at the decadal time scale. *J. Phys. Oceanogr.* 35, 2467–2486.
- Jackett, D.R., McDougall, T.J., 1995. Minimal adjustment of hydrographic profiles to achieve static stability. *J. Atmos. Ocean. Technol.* 12, 381–389.
- Josey, S.A., Marsh, R., 2005. Surface freshwater flux variability and recent freshening of the North Atlantic in the eastern subpolar gyre. *J. Geophys. Res.* 110, C05008.
- Latif, M., Roeckner, E., Mikolajewicz, U., Voss, R., 2000. Tropical stabilization of the thermohaline circulation in a greenhouse warming simulation. *J. Clim.* 13, 1809–1813.
- Levitus, S., 1982. *Climatological atlas of the world ocean*. Technical report. National Oceanic and Atmospheric Administration. NOAA Professional Paper 13.
- Lukas, R., 2001. Freshening of the upper thermocline in the North Pacific subtropical gyre associated with decadal changes of rainfall. *Geophys. Res. Lett.* 28 (18), 3485–3488.
- Madec, G., Imbard, M., 1996. A global ocean mesh to overcome the North Pole singularity. *Clim. Dyn.* 12 (6), 381–388.
- Madec, G., Delecluse, P., Imbard, M., & Levy, C., 1998. OPA Version 8.1 Ocean General Circulation Model reference manual. LODYC/IPSL Technical report 11.
- Maes, C., Picaut, J., Belamari, S., 2002. Salinity barrier layer and onset of El Niño in a Pacific coupled model. *Geophys. Res. Lett.* 29 (24).
- Maes, C., Picaut, J., Belamari, S., 2005. Importance of the salinity barrier layer for the buildup of El Niño. *J. Clim.* 18 (1), 104–118.
- Manabe, S., Stouffer, R., 1995. Simulation of abrupt climate change induced by freshwater input to the North Atlantic ocean. *Nature* 378 (6553), 165–167.
- Marsland, S.J., Wolff, J.-O., 2001. On the sensitivity of Southern Ocean sea ice to the surface freshwater flux: a model study. *J. Geophys. Res.* 106 (C2), 2723–2741.
- Martinson, D.G., 1990. Evolution of the southern ocean winter mixed layer and sea ice: open ocean deepwater formation and ventilation. *J. Geophys. Res.* 95 (C7), 11641–11654.
- Martinson, D.G., Iannuzzi, R.A., 1998. Antarctic ocean–ice interactions: implications from ocean bulk property distributions in the Weddell gyre. In: Jeffries, M.O. (Ed.), *Antarctic Sea Ice: Physical Processes, Interactions and Variability*, volume 74 of Antarctic Research Series. American Geophysical Union, Washington, DC, pp. 243–271.
- Murray, R.J., 1996. Explicit generation of orthogonal grids for ocean models. *J. Comp. Phys.* 126 (2), 251–273.
- Oka, A., Hasumi, H., 2004. Effects of freshwater forcing on the Atlantic deep circulation: a study with an OGCM forced by two different surface freshwater flux datasets. *J. Clim.* 17 (11), 2180–2194.
- Osborn, T.J., 1998. The vertical component of epineutral diffusion and the dianeutral component of horizontal diffusion. *J. Phys. Oceanogr.* 28, 485–494.
- Rahmstorf, S., 1996. On the freshwater forcing and transport of the Atlantic thermohaline circulation. *Clim. Dyn.* 12, 799–811.
- Roeckner, E., et al., 1996. The atmospheric general circulation model ECHAM-4: model description and simulation of present-day climate. Max-Planck-Institut für Meteorologie report number 218.

- Roulet, G., Madec, G., 2000. Salt conservation, free surface, and varying levels: a new formulation for ocean general circulation models. *J. Geophys. Res. Oceans* 105, 23927–23942.
- Saenko, O.A., Gregory, J.M., Weaver, A.J., Eby, M., 2002. Distinguishing the influence of heat, freshwater, and momentum fluxes on ocean circulation and climate. *J. Clim.* 15 (24), 3686–3697.
- Schmitt, R.W., 1995. The ocean component of the global water cycle. *Rev. Geophys.* 33, 1395–1409.
- Spigel, R.H., Priscu, J.C., 1996. Evolution of temperature and salt structure of Lake Bonney, a chemically stratified Antarctic lake. *Hydrobiologia* 321 (3), 177–190.
- Stott, P.A., Sutton, R.T., Smith, D.M., 2008. Detection and attribution of Atlantic salinity changes. *Geophys. Res. Lett.* 35, L21702.
- Swingedouw, D., Braconnot, P., Delecluse, P., Guilyardi, E., Marti, O., 2007. The impact of global freshwater forcing on the thermohaline circulation: adjustment of North Atlantic convection sites in a CGCM. *Clim. Dyn.* 28, 291–305.
- Thorpe, R.B., Gregory, J.M., Johns, T.C., Wood, R.A., Mitchell, J.F.B., 2001. Mechanisms determining the Atlantic thermohaline circulation response to greenhouse gas forcing in a non-flux-adjusted coupled climate model. *J. Clim.* 14 (14), 3102–3116.
- Timmermann, R., Goosse, H., Madec, G., Fichefet, T., Ethe, C., Dulière, V., 2005. On the representation of high latitude processes in the ORCA-LIM global coupled sea ice-ocean model. *Ocean Model.* 8, 175–201.
- Valcke, S., Terray, L., Piacentini, A., 2000. The OASIS coupler user guide Version 2.4. Technical report TR/CMGC/00-10, CERFACS.
- Vellinga, M., Wood, R., Gregory, J., 2002. Processes governing the recovery of a perturbed thermohaline circulation in HadCM3. *J. Clim.* 15 (7), 764–780.
- Vialard, J., Delecluse, P., 1998a. An OGCM study for the TOGA decade. Part I. Role of salinity in the physics of the western Pacific fresh pool. *J. Phys. Oceanogr.* 28, 1071–1088.
- Vialard, J., Delecluse, P., 1998b. An OGCM study for the TOGA decade. Part II. Barrier-layer formation and variability. *J. Phys. Oceanogr.* 28, 1089–1106.
- Vialard, J., Delecluse, P., Menkes, C., 1993. A modelling study of salinity variability and its effects in the tropical Pacific ocean during the 1999 period. *J. Geophys. Res.* 107, 8005.
- Wang, X., Stone, P.H., Marotzke, J., 1999a. Global thermohaline circulation. Part I. Sensitivity to atmospheric moisture transport. *J. Clim.* 12 (1), 71–82.
- Wang, X., Stone, P.H., Marotzke, J., 1999b. Global thermohaline circulation. Part II. Sensitivity with interactive atmospheric transports. *J. Clim.* 12 (1), 83–91.
- Williams, P.D., Guilyardi, E., Sutton, R.T., Gregory, J.M., Madec, G., 2006. On the climate response of the low-latitude Pacific ocean to changes in the global freshwater cycle. *Clim. Dyn.* 27 (6), 593–611.
- Williams, P.D., Guilyardi, E., Sutton, R.T., Gregory, J.M., Madec, G., 2007. A new feedback on climate change from the hydrological cycle. *Geophys. Res. Lett.* 34, L08706.
- Wong, A.P.S., Bindoff, N.L., Church, J.A., 1999. Large-scale freshening of intermediate waters in the Pacific and Indian oceans. *Nature* 400, 440–443.
- Wood, R.A., Keen, A.B., Mitchell, J.F.B., Gregory, J.M., 1999. Changing spatial structure of the thermohaline circulation in response to atmospheric CO₂ forcing in a climate model. *Nature* 399, 572–575.
- Yang, F., Kumar, A., Schlesinger, M.E., Wang, W., 2003. Intensity of hydrological cycles in warmer climates. *J. Clim.* 16, 2419–2423.